Electronic Supplementary Material (ESI) for ChemComm.
This journal is © The Royal Society of Chemistry 2020

Supporting Information for

Passing the framework skeleton and properties of coordination material on to organic framework material

Xuan Wang, Ming-Jie Dong, Kai Chen, Zi-Kun Liu and Chuan-De Wu*

1. Experimental Section

Materials and Methods

All chemicals were obtained from commercial sources and were used without further purification, except tetrakis 3,5-bis((4-hydroxycarbonyl)-phenyl)phenylporphine (H_{10}**L**) was synthesized according to the literature.[S1] Powder X-ray diffraction (PXRD) patterns were recorded on a RIGAKU D/MAX 2550/PC for Cu Kα radiation (λ = 1.5406 Å) with a scan speed of 1 °/min and a step size of 0.02° in 2θ. Fourier transform infrared spectra (FT-IR) were collected from KBr pellets on a Nicolet NEXUS 470 spectrometry in the range of 400-4000 cm^{-1}. UV-visible absorption spectra were obtained on a UV-visible spectrophotometer (TU-1901, PERSEE). UV-visible diffuse reflectance spectra were collected using the same spectrophotometer equipped with an integrated sphere, and $BaSO_4$ was used as a reference for the measurements. Thermogravimetric-mass spectrometry (TG-MS) experiments were carried out on a TGA/DSC1 1100S (Mettler-Toledo) coupled with a ThermoStar GSD320 mass spectrometry (Pfeiffer Vacuum), and the heating rate is of 10 °C/min under 1 atm N_2 atmosphere. Matrix-assisted laser desorption/ionization time-of-flight mass spectrometry (MALDI-TOF MS) experiments were performed on a Bruker UltrafleXtreme™ mass spectrometer equipped with a modified Nd: YAG laser (355 nm, 2000 Hz). X-ray photoelectron spectra (XPS) were measured by a Thermo ESCALAB 250Xi with Al-Kα irradiation (1486.6 eV), and the binding energies were calibrated using the C1s peak at 284.8 eV. Raman spectra were obtained using a Raman spectrometer (Horiba Co., Lab HR800) with an Ar laser of

532 nm as the excitation wavelength. The CO_2 sorption isotherms were performed on a Micromeritics ASAP 2020 surface area analyzer at 195 and 273 K. The samples were degassed in vacuum at 80 ^oC for 12 h prior to analysis. Scanning electron microscopy (SEM) images were recorded on a Hitachi SU8010 equipment equipped with an energy dispersive X-ray (EDX) detector. Transmission electron microscopy (TEM) images were recorded using a Hitachi HT-7700 electron microscope. High resolution transmission electron microscopy (HRTEM) images were recorded on a JEM 2100F equipment. GC-MS data were recorded on a SHIMADZU GCMS-QP2010. Inductively coupled plasma optical emission spectrometry (ICP-OES) was performed on a Varian 730-ES spectrometer. The water contact angles were observed using sessile method on a Dataphysics OCA20 system at room temperature.

Synthesis of CZJ-6

CZJ-6 was synthesized according to the literature.[S1] H_{10}**L** (10 mg, 0.006 mmol) and $Cu(OAc)_2 \cdot H_2O$ (15 mg, 0.075 mmol) were dissolved in a mixture of DMF (16 mL) and dilute HNO_3 (4 M, 3 mL). The reaction solution was sealed in a screw cap vial and heated at 80 °C for one week. Brown crystals of CZJ-6 were collected by filtration, washed with DMF, EtOH and Et_2O, and dried at room temperature. Yield: 80% (based on H_{10}**L**). FT-IR (KBr pellet, ν/cm^{-1}): 2956(w), 2920(w), 1701(w), 1608(s), 1588(s), 1538(m), 1401(s), 1016(w), 1004(w), 856(w), 782(m), 747(w), 708(w), 670(w).

Synthesis of OFM-1

CZJ-6 (20 mg, 0.006 mmol), K_2CO_3 (1.4 mg, 0.010 mmol), H_2O (0.1 mL) and CH_3CN (3.0 mL) were mixed in a 5-mL Teflon-lined stainless steel container. 1,2,4,5-tetrakis(bromomethyl)benzene (6.0 mg, 0.013 mmol) was added into the mixture, and then the container was sealed and heated at 120 °C in an oven for 3 days. Dark purple solid of OFM-1 was collected by filtration, washed with 0.1 M HCl aqueous solution, DMF, THF and Et_2O, and dried at room temperature. Yield: 91%. FT-IR (KBr pellet, ν/cm^{-1}): 2956(w), 2920(w), 1720(s), 1607(s), 1592(m), 1437(w), 1377(m), 1268(s), 1102(s), 1017(m), 1004(w), 852(w), 769(m), 740(w), 702(w), 670(w).

Synthesis of benzene-1,2,4,5-tetrayltetrakis(methylene) tetrabenzoate

1,2,4,5-tetrakis(bromomethyl)benzene (45.0 mg, 0.10 mmol) was dissolved in 4 mL of CH_3CN, and K_2CO_3 (22.1 mg, 0.16 mmol), copper benzoate (122.3 mg, 0.40 mmol) and H_2O (0.8 mL) were subsequently added into the solution. The mixture was stirred at 120 °C for 24 h. After cooling to room temperature, the reaction mixture was poured into water. The solid was collected by centrifugation, washed with H_2O and CH_3OH several times, and dried at 80 ^{o}C. The residue was purified by silica gel chromatography (*n*-hexane/$CHCl_3$) to afford white solid. Yield: 95%. ^{1}H NMR (400 MHz, $CDCl_3$) δ_H 8.06-7.98 (m, 8H), 7.72 (s, 2H), 7.53 (t, J = 7.4 Hz, 4H), 7.37 (t, J = 7.8 Hz, 8H), 5.55 (s, 8H). ^{13}C NMR (400 MHz, $CDCl_3$) δ_C 166.2, 135.2, 133.2, 131.2, 129.7, 128.4, 63.9.

Synthesis of 5,10,15,20-tetrakis-3,5-bis((4-benzyloxycarbonyl)phenyl)

phenylporphine (TBPP)

H_{10}**L** (50 mg, 0.03 mmol), K_2CO_3 (199 mg, 1.44 mmol) and benzyl bromide (342 mg, 2.0 mmol) were dissolved in 3 mL of DMF. The mixture was stirred at 100 °C for 12 h. After cooling to room temperature, the reaction mixture was poured into aqueous hydrochloric acid solution (pH = 1), and thoroughly extracted by CH_2Cl_2 solvent. The CH_2Cl_2 layer was separated, and successively washed with H_2O and saturated NaCl aqueous solution. The CH_2Cl_2 layer was dried with anhydrous Na_2SO_4 and concentrated under reduced pressure, and the resulting residue was purified by silica gel chromatography (*n*-hexane/CH_2Cl_2) to afford purple solid. Yield: 63%. ^{1}H NMR (400 MHz, CDCl3) δ_H 9.04 (s, 8H), 8.55 (d, J = 1.6 Hz, 8H), 8.29 (t, J = 1.6 Hz, 4H), 8.21 (d, J = 8.5 Hz, 16H), 7.96 (d, J = 8.5 Hz, 16H), 7.47-7.42 (m, 16H), 7.40-7.30 (m, 24H), 5.38 (s, 16H), 2.64 (s, 2H). ^{13}C NMR (400 MHz, CDCl3) δ_C 166.20, 145.03, 143.45, 139.31, 136.02, 133.16, 130.55, 129.58, 128.65, 128.33, 128.22, 127.59, 125.81, 119.69, 66.85.

Synthesis of CZJ-6(t)

CZJ-6 (20 mg, 0.006 mmol), K_2CO_3 (1.4 mg, 0.010 mmol), H_2O (0.1 mL) and CH_3CN (3.0 mL) were mixed in a 5-mL Teflon-lined stainless steel container. 1,2,4,5-tetrakis(bromomethyl)benzene (6.0 mg, 0.013 mmol) was added into the mixture, and then the container was sealed and heated at 120 °C in an oven for appropriate time. Dark purple solid was collected by filtration, washed with CH_3CN and Et_2O, and dried at room temperature, affording CZJ-6(t), where t represents the

reaction time.

Synthesis of CZJ-6(t)-MS

CZJ-6(t) (10 mg) was soaked in 2 mL of hydrochloric acid aqueous solution (pH = 1) and vigorously stirred for 24 h. The solid was collected by filtration and washed with H_2O several times, and dried at 100 °C for 6 h. The solid was added into 1 mL of THF solvent under stirring for 1 h, and the supernate was collected by centrifugation, denoted as CZJ-6(t)-MS.

Synthesis of Pd@OFM-1

OFM-1 (50 mg) was thoroughly dispersed in 2.5 mL of CH_2Cl_2 under ultrasonication conditions at room temperature. A palladium acetate solution (10 mg of $Pd(OAc)_2$ in 2.5 mL of CH_2Cl_2) was dropwise added into the above suspension under vigorous stirring at room temperature, and further reacted for 24 h. The solid was collected by centrifugation, washed with dichloromethane several times, and dried under vacuum at 50 ^oC for 6 h. The solid sample was reduced under a stream of H_2/N_2 mixture at 150 ^oC for 2 h to afford Pd@OFM-1. Yield: 95%. The Pd content in Pd@OFM-1 is of 6.4 wt% as determined by ICP-OES analysis.

Aqueous phase phenol hydrogenation experiments

Phenol (0.1 mmol), catalyst (3 μmol, based on Pd), $AlCl_3 \cdot 6H_2O$ (0.01 mmol) and deionized water (1 mL) were fed into a stainless steel autoclave. The autoclave was sealed and purged by 1.0 MPa H_2 three times, and subsequently heated at 90 °C under

stirring for 24 h. After cooling to room temperature, the mixture was extracted with ethyl acetate, and analyzed by gas chromatography. The solid catalyst was recovered by centrifugation, thoroughly washed with ethyl acetate and methanol several times. After drying in vacuum at 50 ^{o}C for 6 h, the solid catalyst was reduced under H_2/N_2 atmosphere at 150 °C for 2 h, and reused in the next catalytic run.

2. Supplemental Figures

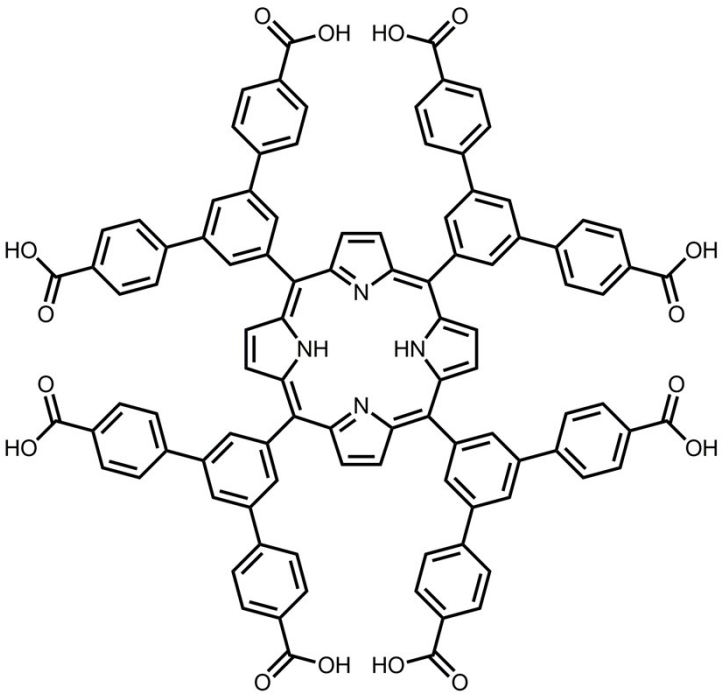

Scheme S1. The structure of tetrakis-3,5-bis((4-hydroxycarbonyl)-phenyl) phenylporphine (H_{10}**L**).

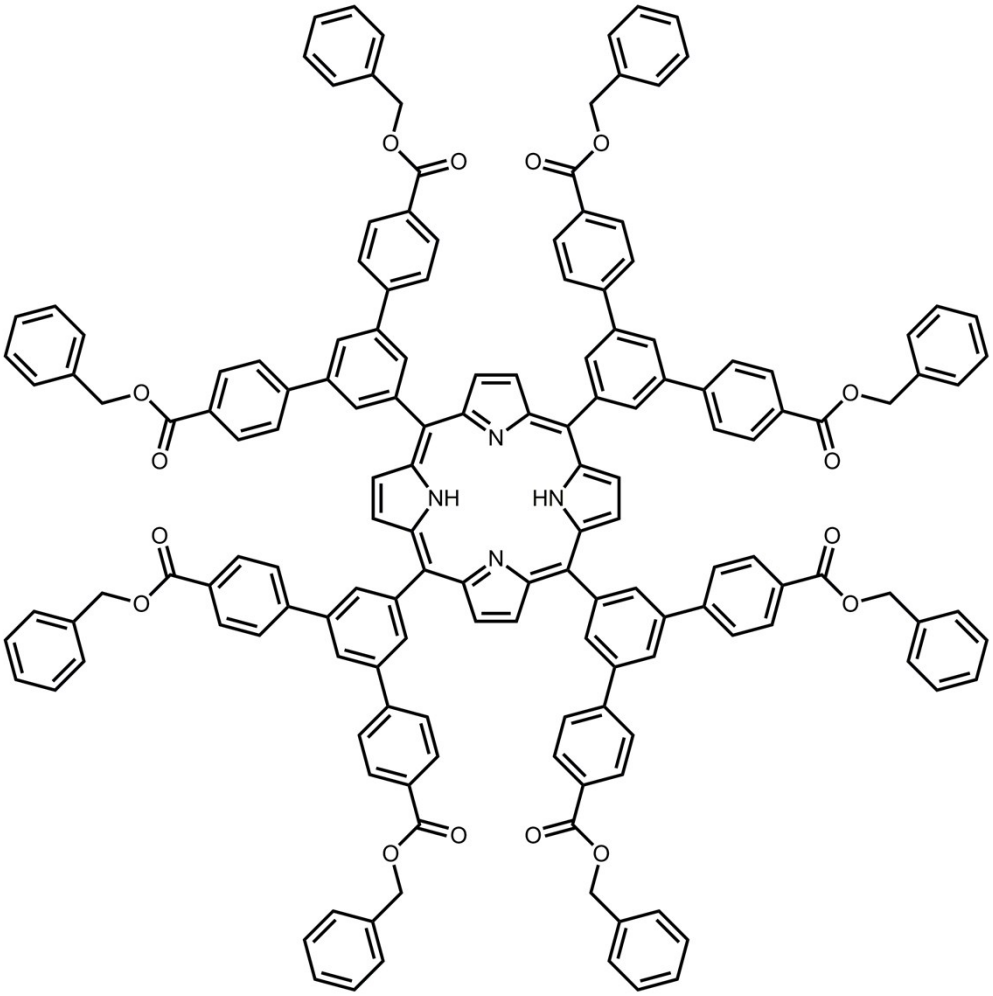

Scheme S2. The structure of 5,10,15,20-tetrakis-3,5-bis((4-benzyloxycarbonyl)phenyl) phenylporphine (TBPP).

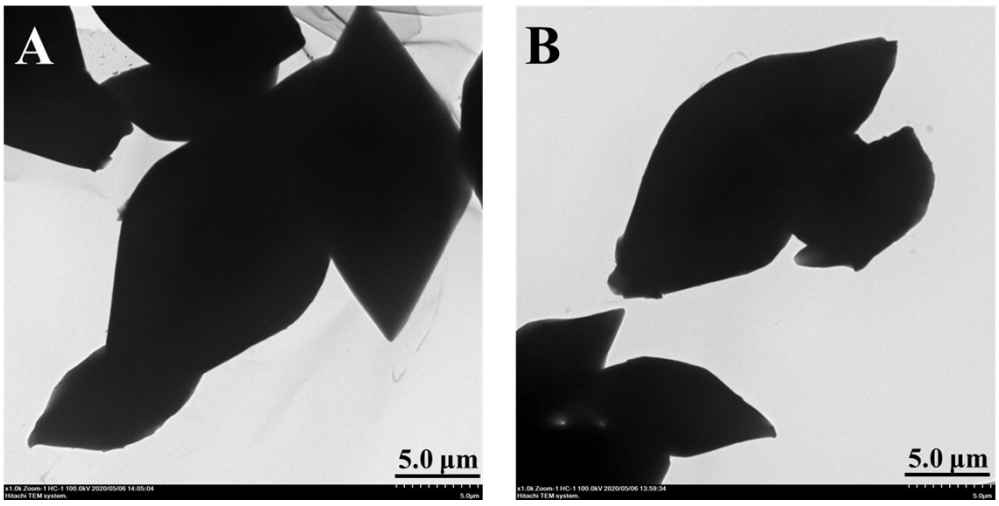

Fig. S1. TEM images of (A) CZJ-6 and (B) OFM-1.

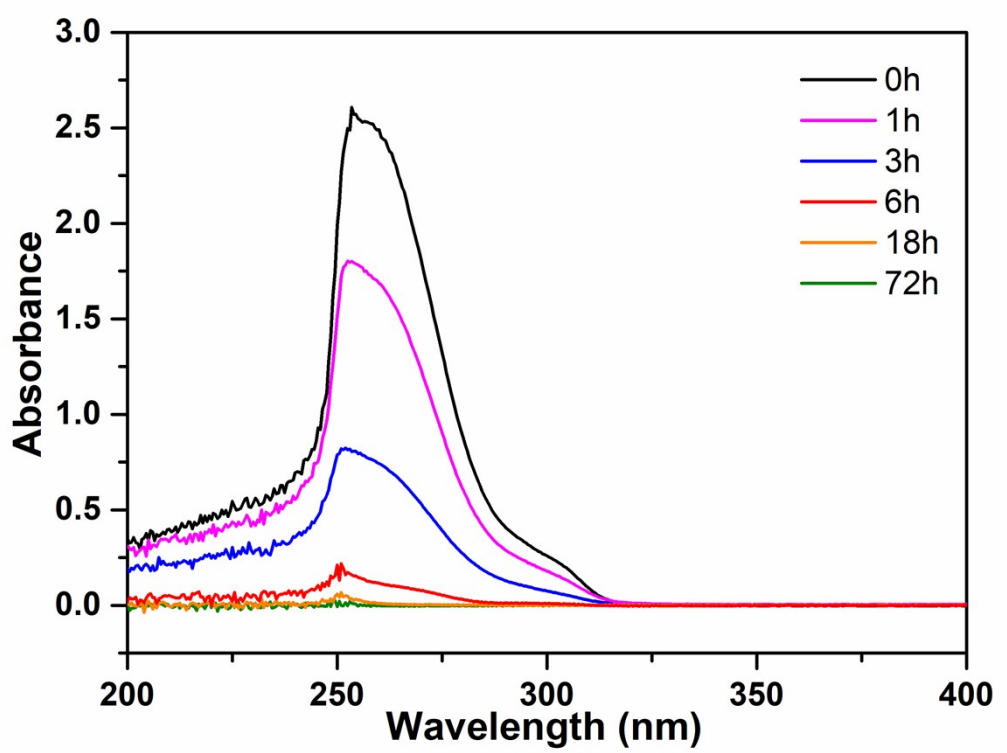

Fig. S2. UV-vis absorption spectra of TBMB during transformation of CZJ-6 into OFM-1 at different reaction times. When the reaction was proceeded for a certain time, the reaction was intentionally interrupted by cooling to room temperature. The supernates were collected and concentrated under reduced pressure. The resulting residue was eluted with CH_2Cl_2 by silica gel chromatography, concentrated under reduced pressure, dissolved in ethyl acetate, and used for UV-vis absorption spectroscopy measurement.

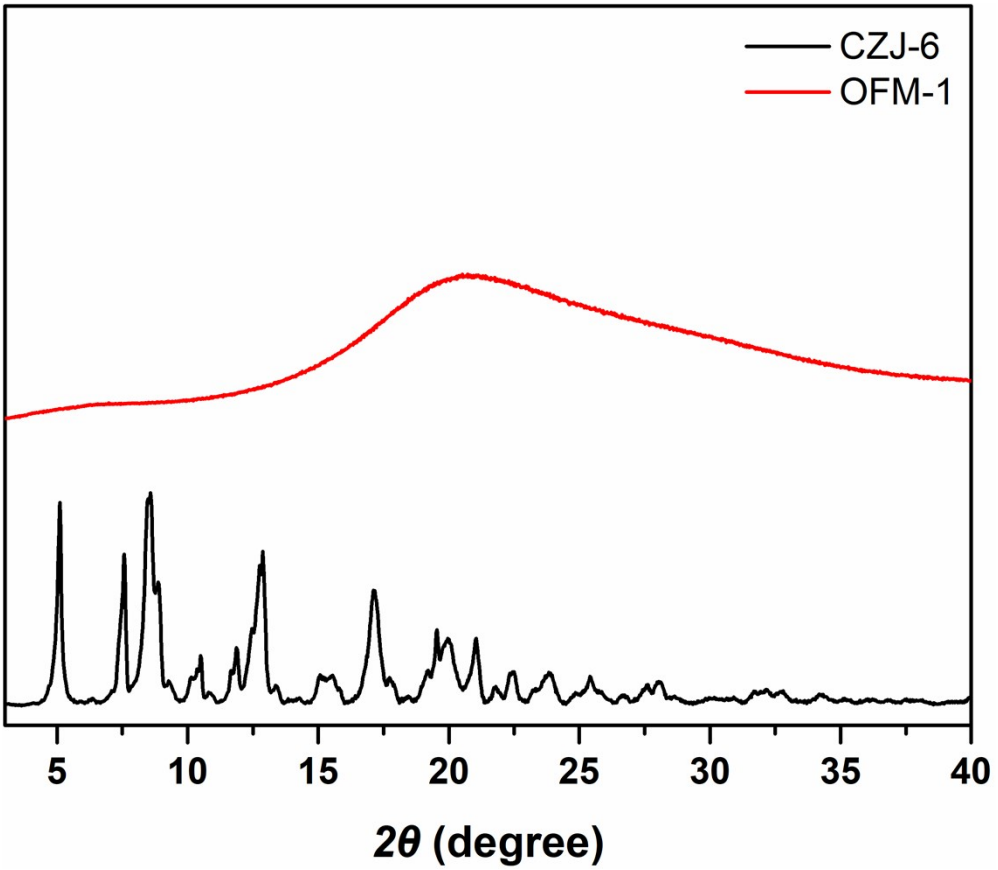

Fig. S3. PXRD patterns of CZJ-6 and OFM-1.

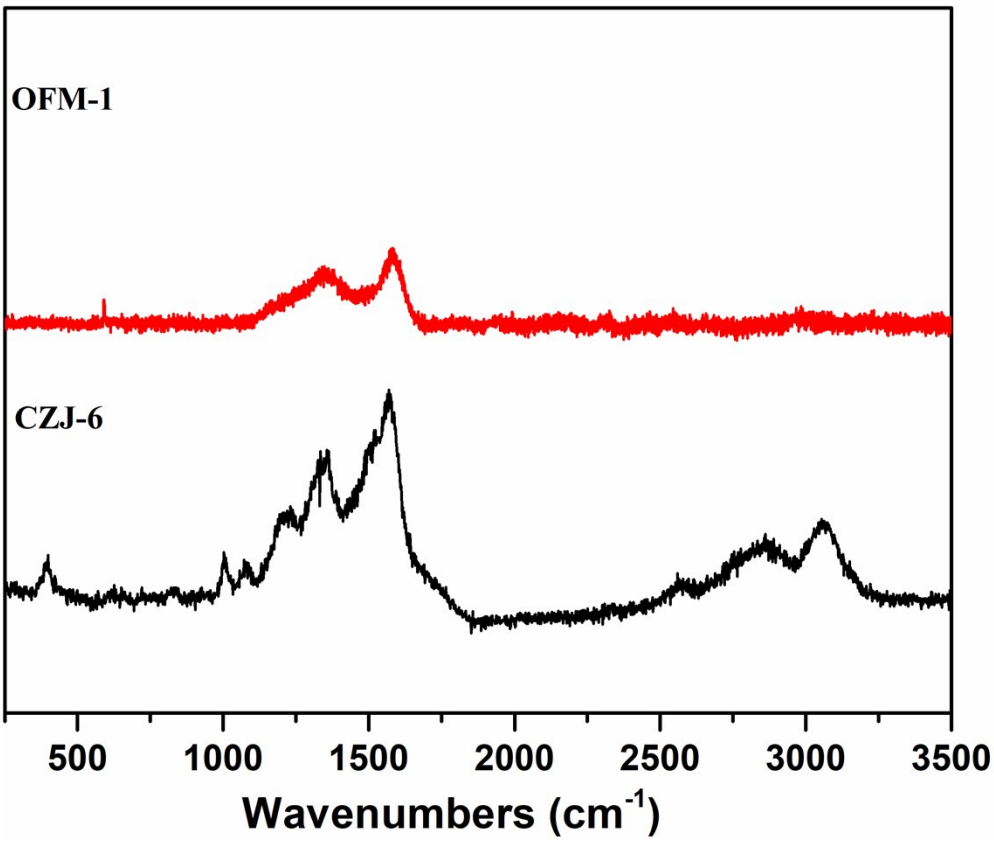

Fig. S4. Raman spectra of CZJ-6 and OFM-1.

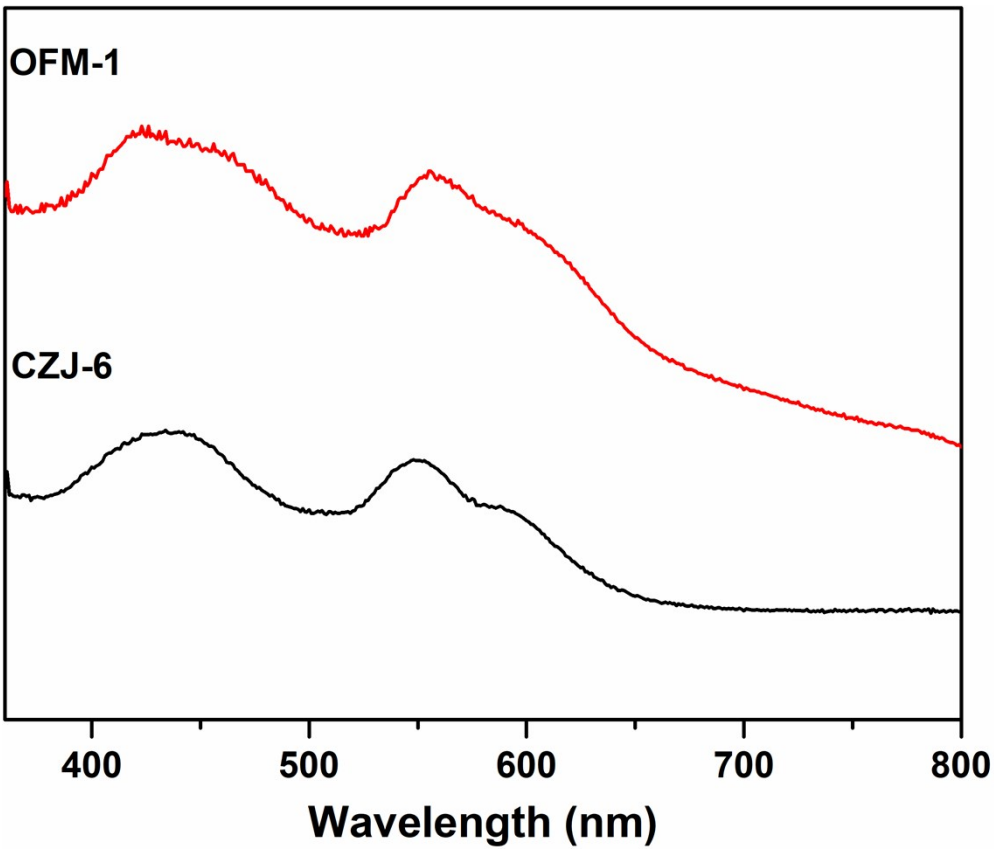

Fig. S5. UV-vis diffuse reflectance spectra of CZJ-6 and OFM-1.

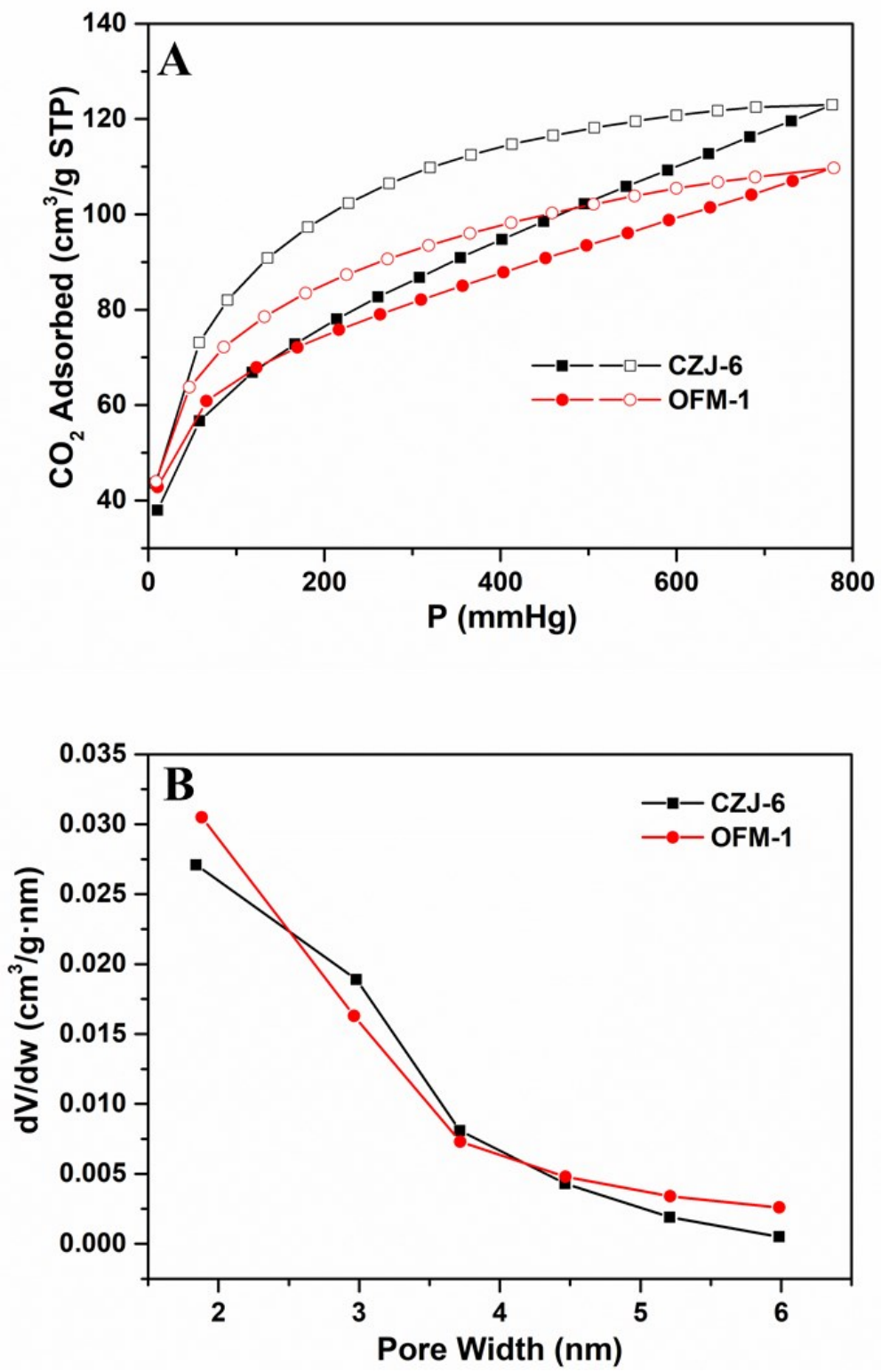

Fig. S6. (A) CO_2 adsorption/desorption isotherms at 195 K and (B) pore size distributions for OFM-1 and CZJ-6.

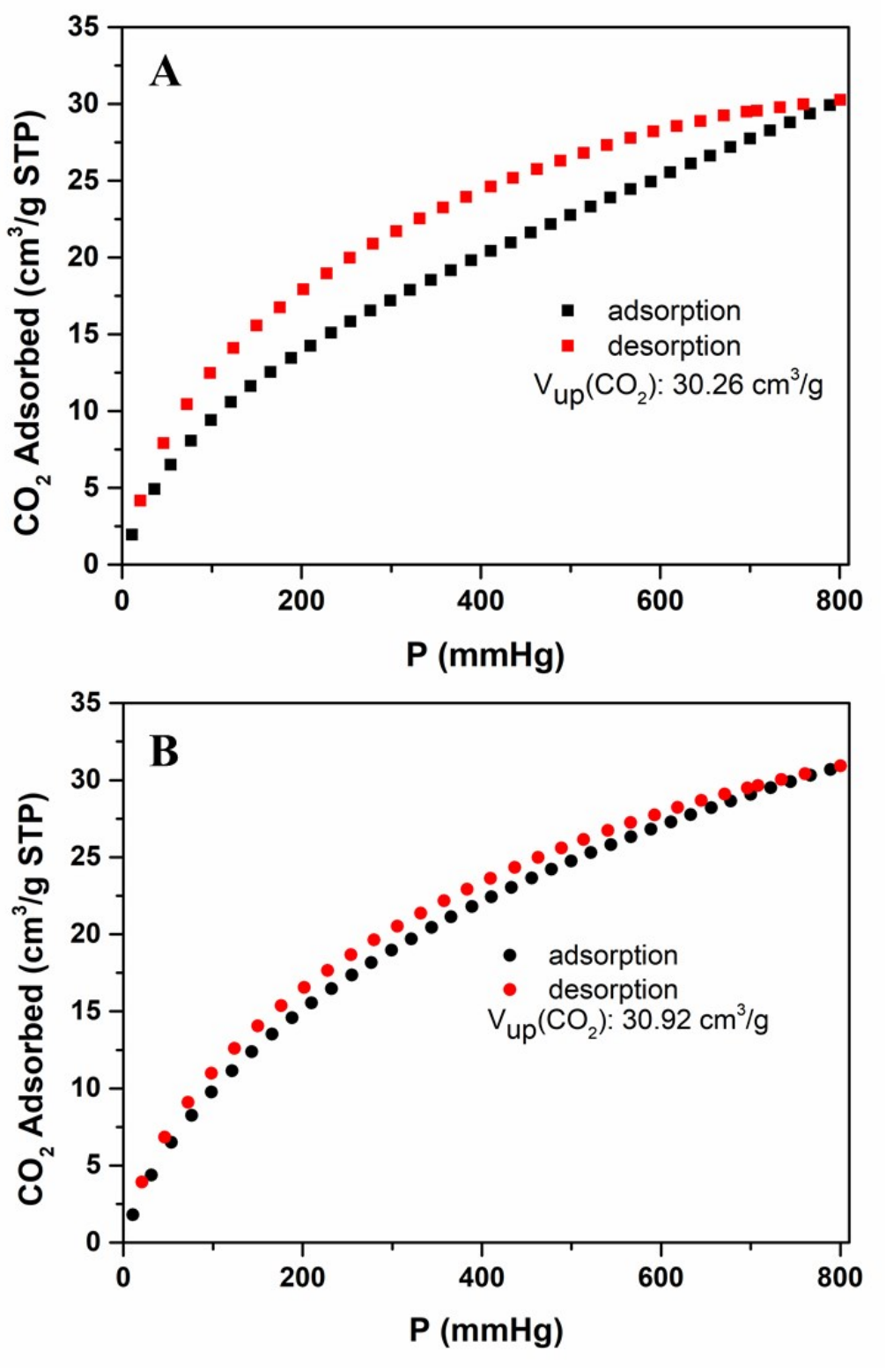

Fig. S7. CO_2 adsorption/desorption isotherms for (A) OFM-1 and (B) CZJ-6 at 273 K.

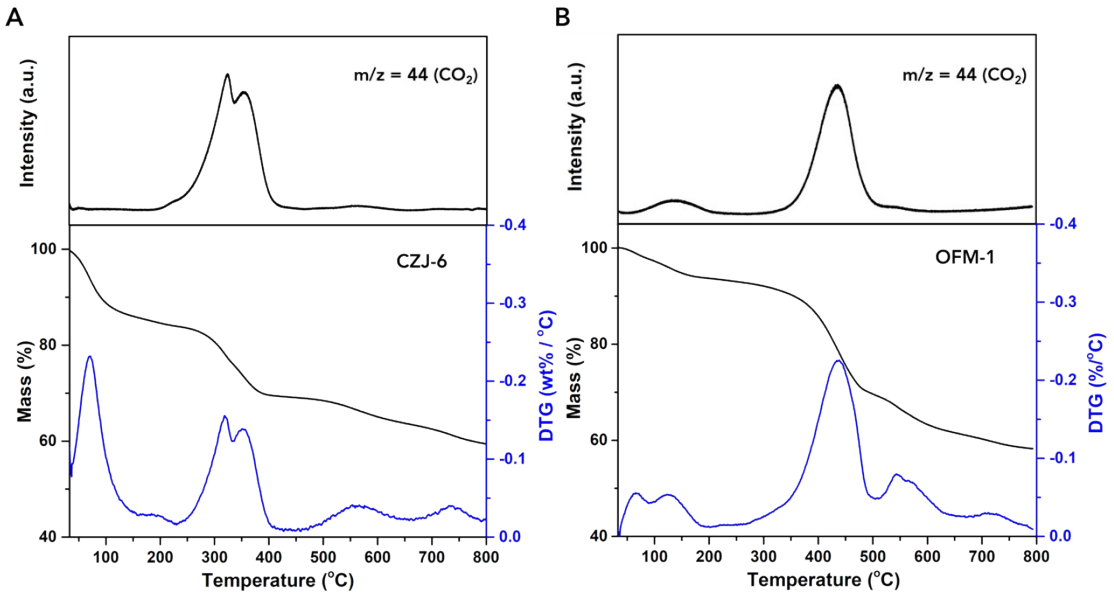

Fig. S8. TG-MS and DTG plots of (A) CZJ-6 and (B) OFM-1.

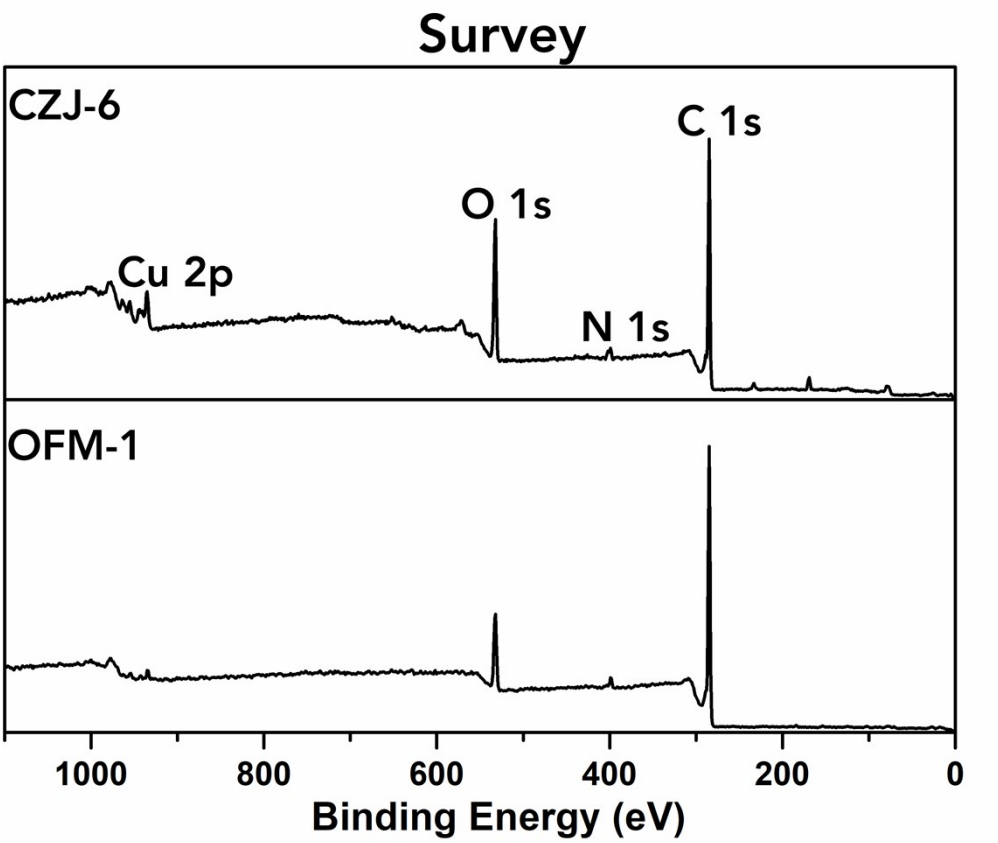

Fig. S9. XPS survey spectra for CZJ-6 and OFM-1.

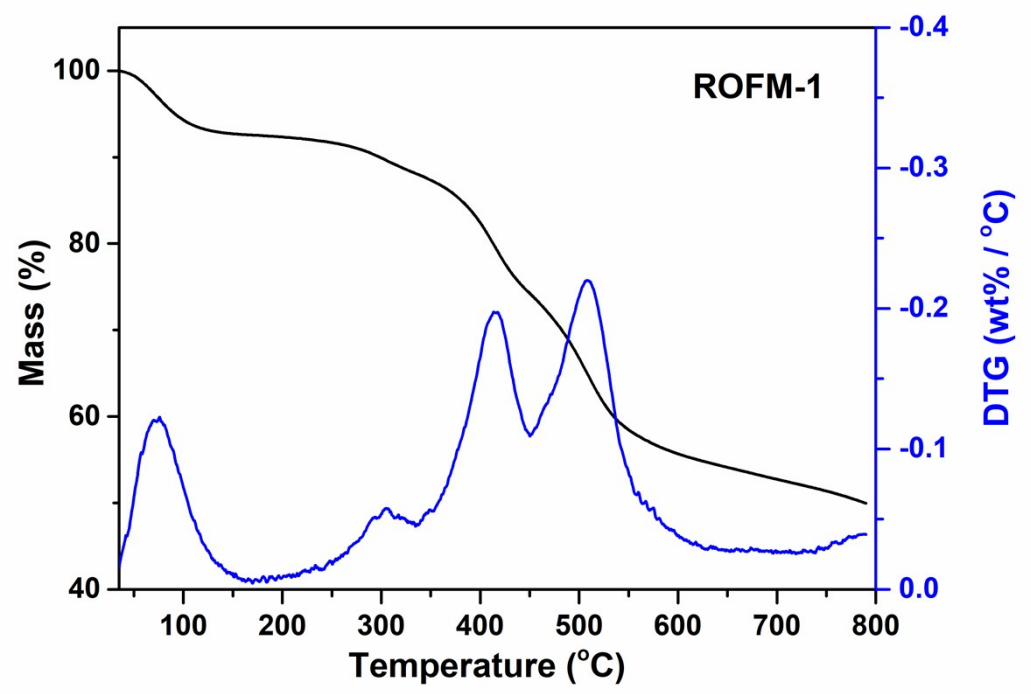

Fig. S10. TG and DTG plots of ROFM-1. ROFM-1 was synthesized according to the following procedure. H_{10}**L** (50 mg, 0.03 mmol), K_2CO_3 (199 mg, 1.44 mmol) and 1,2,4,5-tetrakis(bromomethyl)benzene (27 mg, 0.06 mmol) were dissolved in 3 mL of DMF. The mixture was stirred at 120 °C for 3 days. After cooling to room temperature, the solid was collected by filtration, washed with H_2O and CH_3OH several times, and dried at 80 °C.

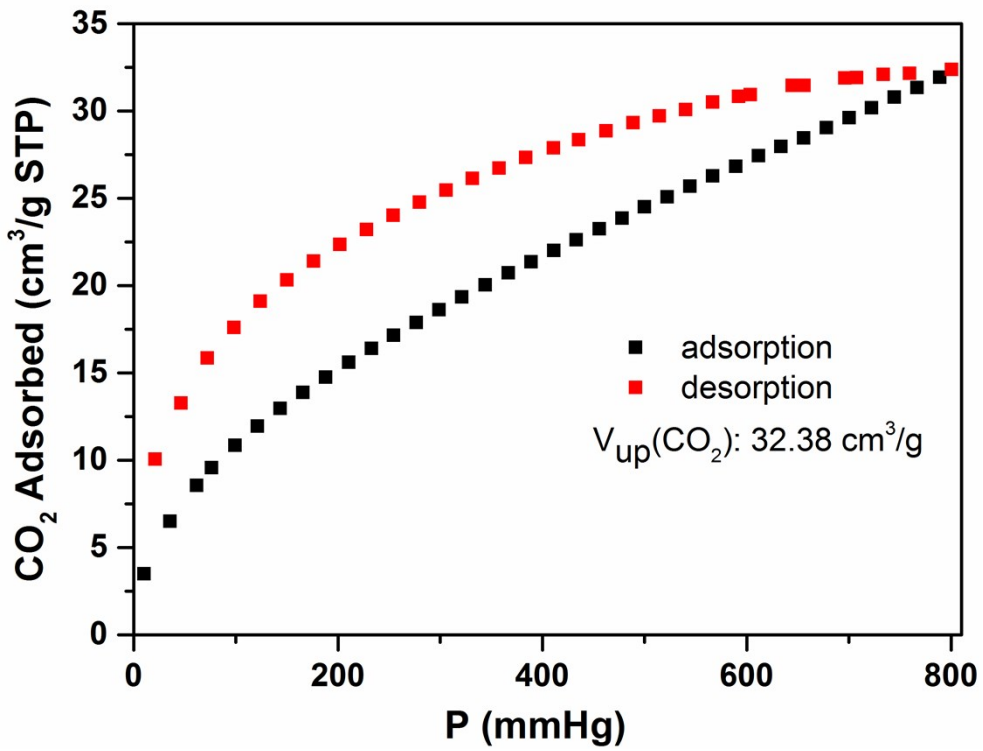

Fig. S11. CO_2 adsorption/desorption isotherms for ROFM-1 at 273 K.

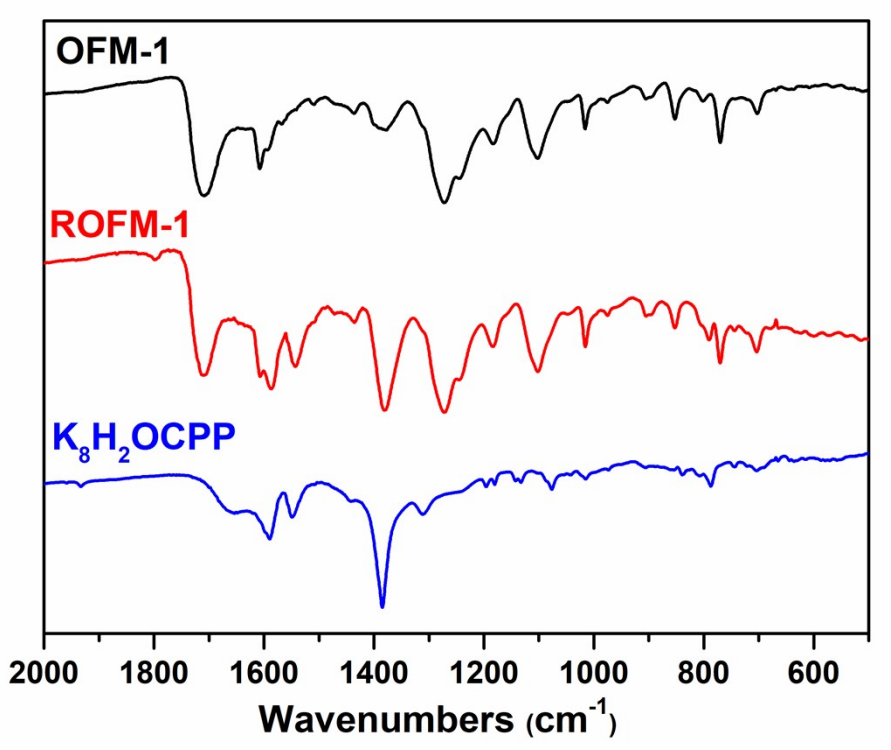

Fig. S12. FT-IR spectra of OFM-1, ROFM-1 and K_8H_2OCPP.

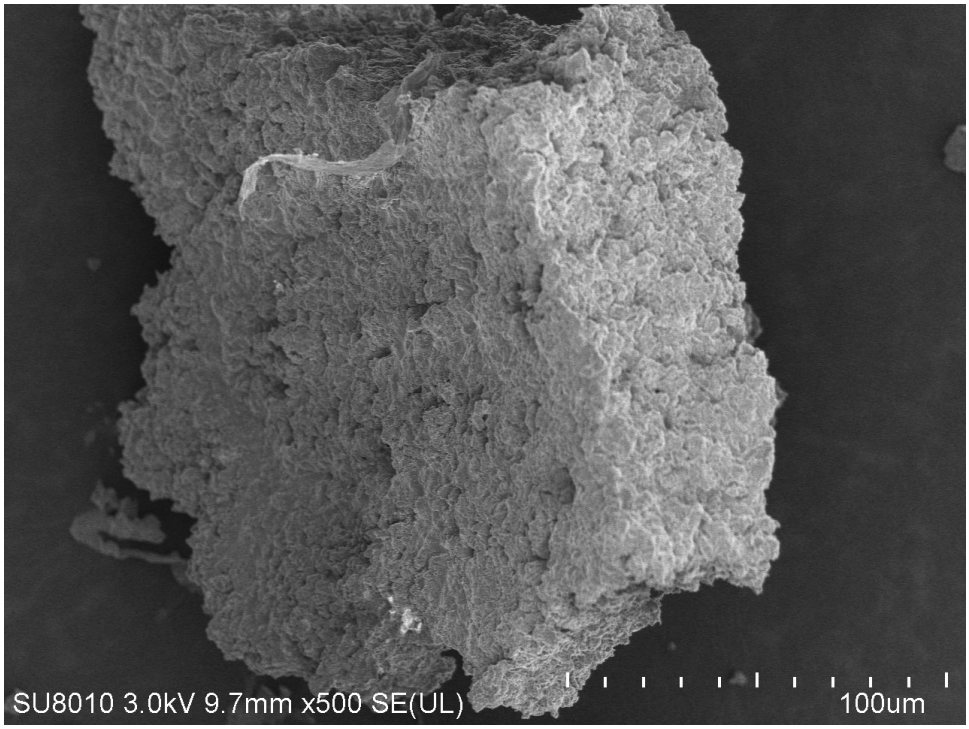

Fig. S13. SEM image of ROFM-1.

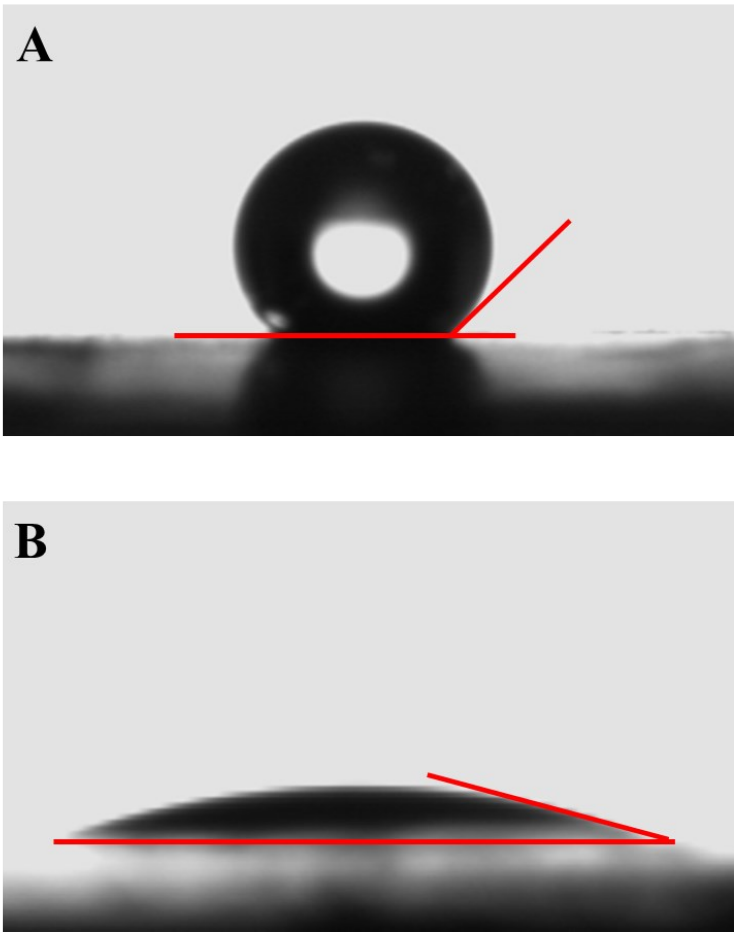

Fig. S14. Static water contact angles of (A) OFM-1 and (B) CZJ-6. CZJ-6 exhibits a hydrophilic water contact angle of 15°, and OFM-1 exhibits a water contact angle of 136°, indicating the hydrophobic nature of OFM-1.

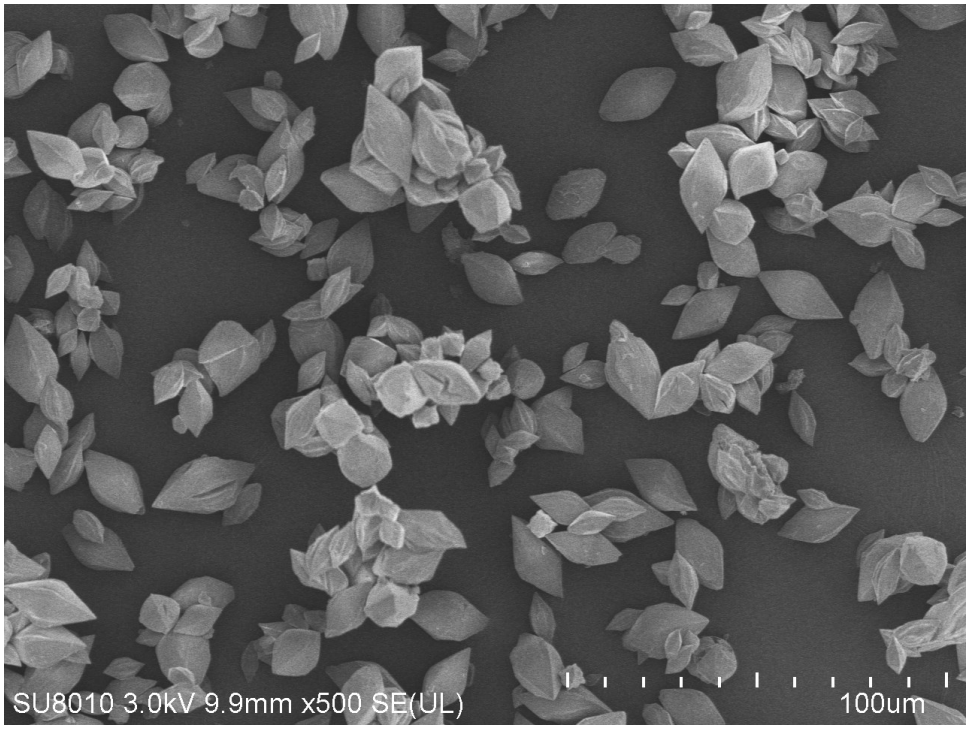

Fig. S15. SEM image of OFM-1 after treating with 6 M hydrochloric acid.

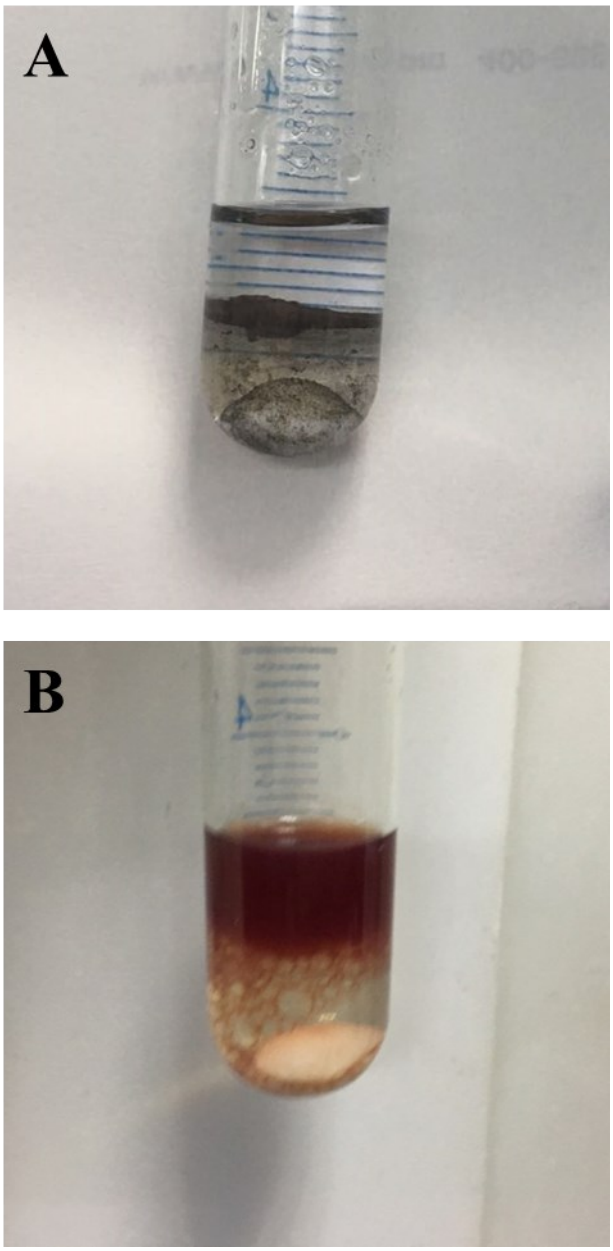

Fig. S16. Digital photographs of (A) OFM-1 and (B) CZJ-6 after hydrochloric acid treatment and subsequent extraction with ethyl acetate.

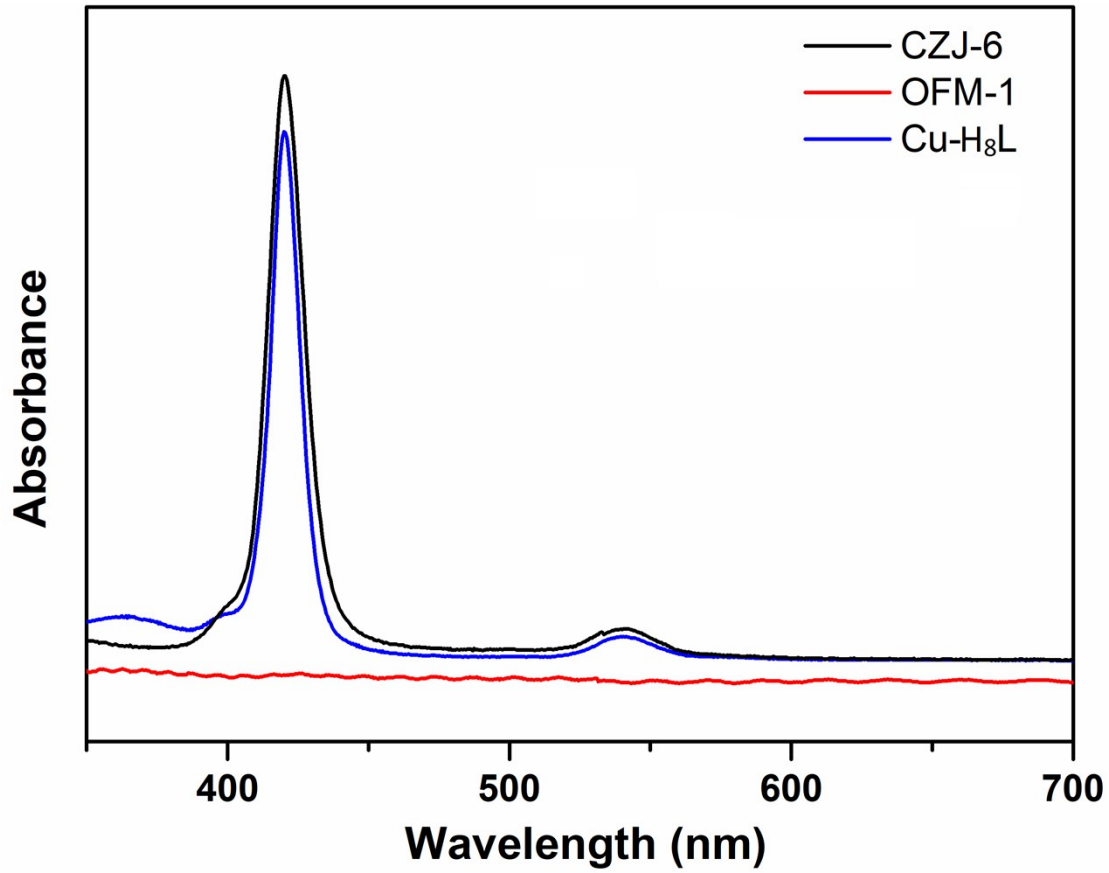

Fig. S17. UV-vis absorption spectra of CZJ-6, OFM-1 and Cu-H_8**L**. After treating with hydrochloric acid and extracted with ethyl acetate several times, the extraction solutions were concentrated under reduced pressure, and the resulting residues were dissolved in DMF.

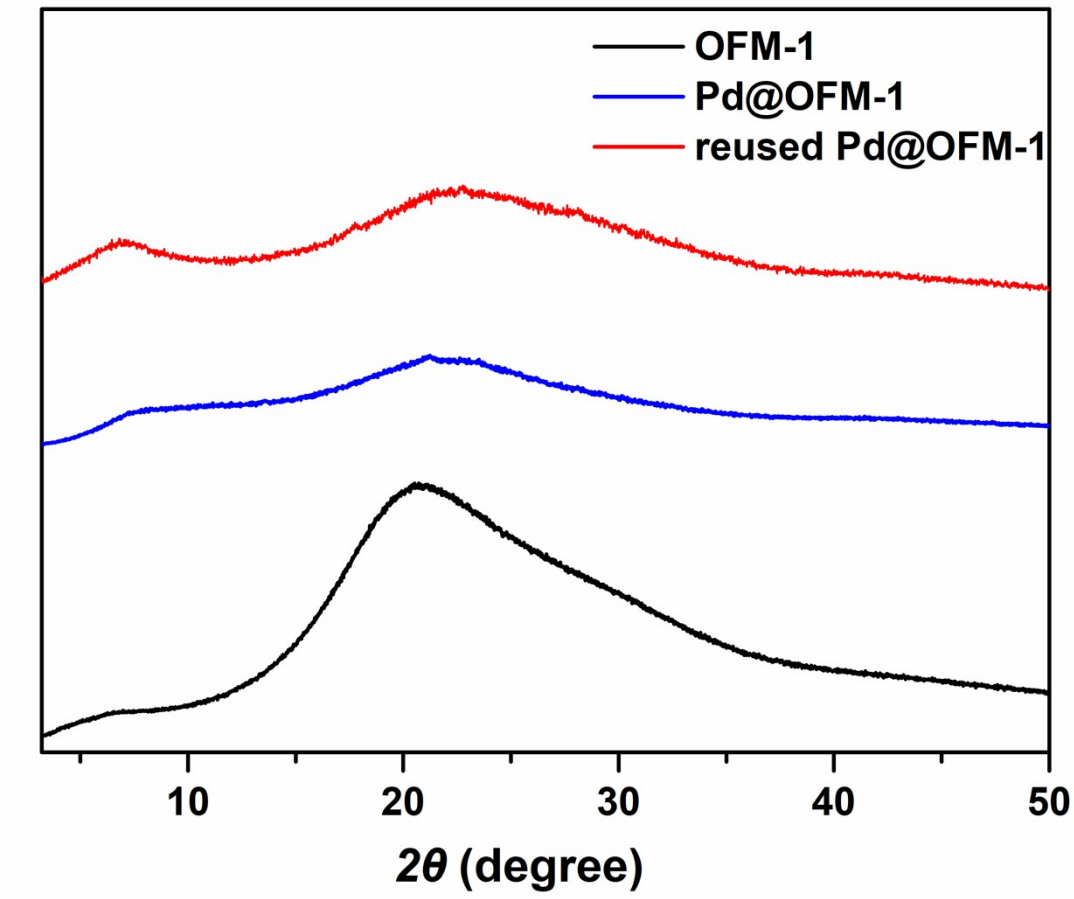

Fig. S18. PXRD patterns of OFM-1, Pd@OFM-1 and reused Pd@OFM-1.

A comparison of the PXRD patterns of OFM-1 and Pd@OFM-1 revealed that no obvious diffraction peak is ascribed to the Pd species, indicating that the sizes of palladium nanoparticles are very small.[S2]

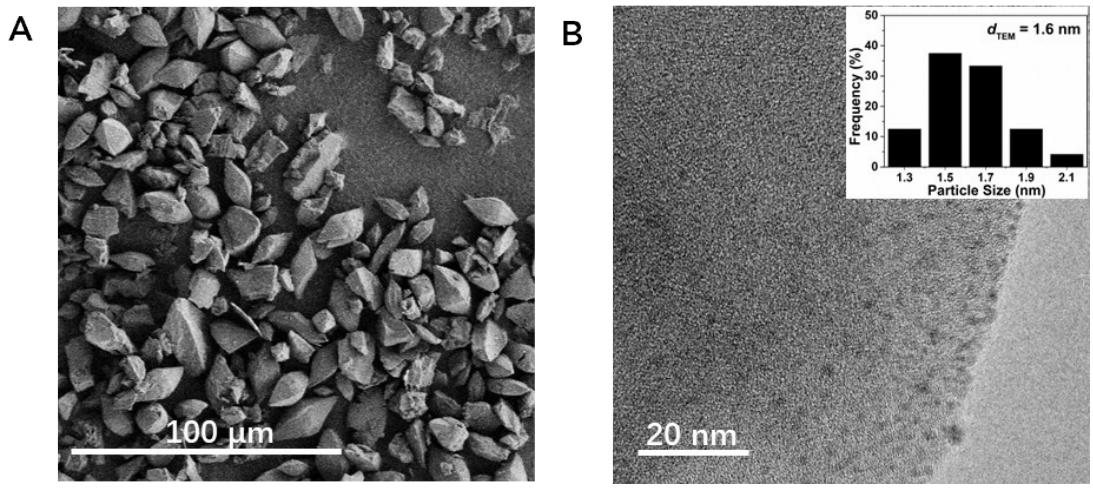

Fig. S19. (A) SEM image and (B) HRTEM image of Pd@OFM-1.

SEM image discloses that Pd@OFM-1 retains the uniform octahedral morphology. High resolution transmission electron microscope (HRTEM) image shows that the palladium species (black dots) are well-dispersed with nanoparticle sizes of ~1.6 nm.

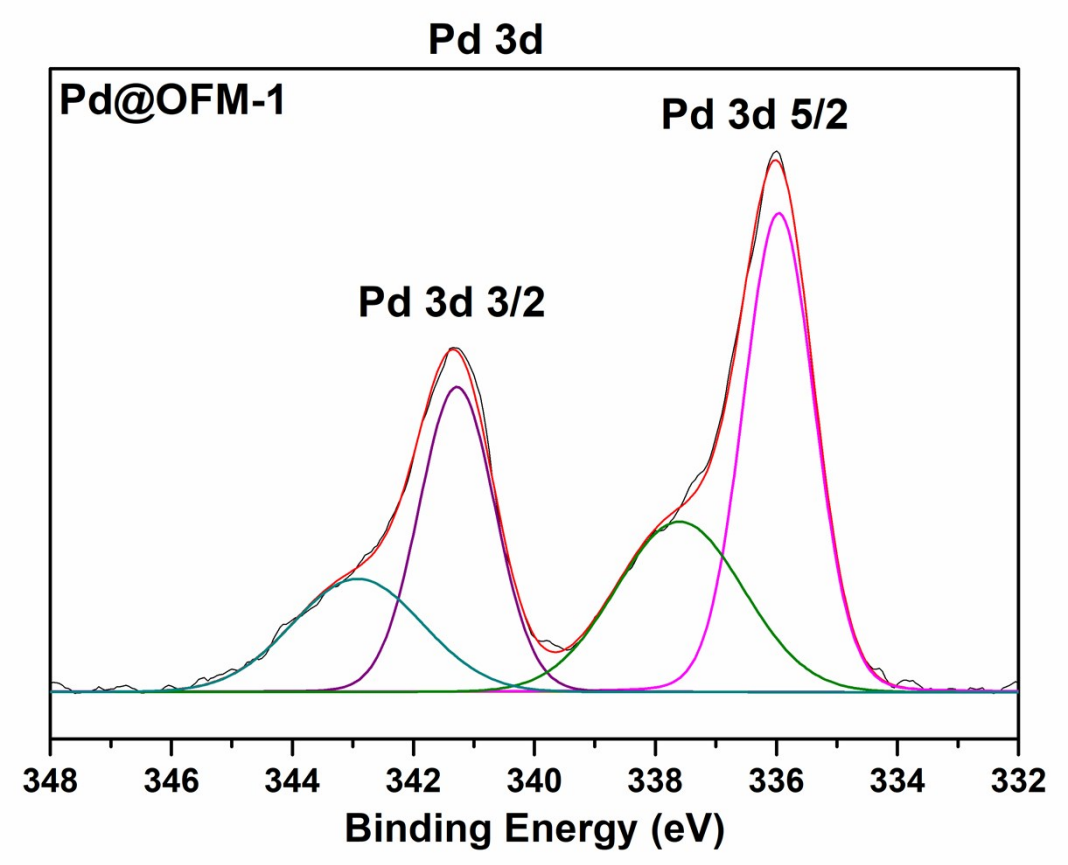

Fig. S20. High resolution Pd 3d XPS spectrum of Pd@OFM-1.

The high resolution Pd 3d XPS spectrum shows the characteristic metallic Pd^0 signals appeared at 341.0 eV ($3d_{3/2}$) and 335.7 eV ($3d_{5/2}$). There also appear the signals at 343.2 eV ($3d_{3/2}$) and 337.9 eV ($3d_{5/2}$) ascribed to the oxidized Pd^{II} species, due to easy reoxidation of the highly dispersed Pd^0 nanoparticles exposed in air.[S3]

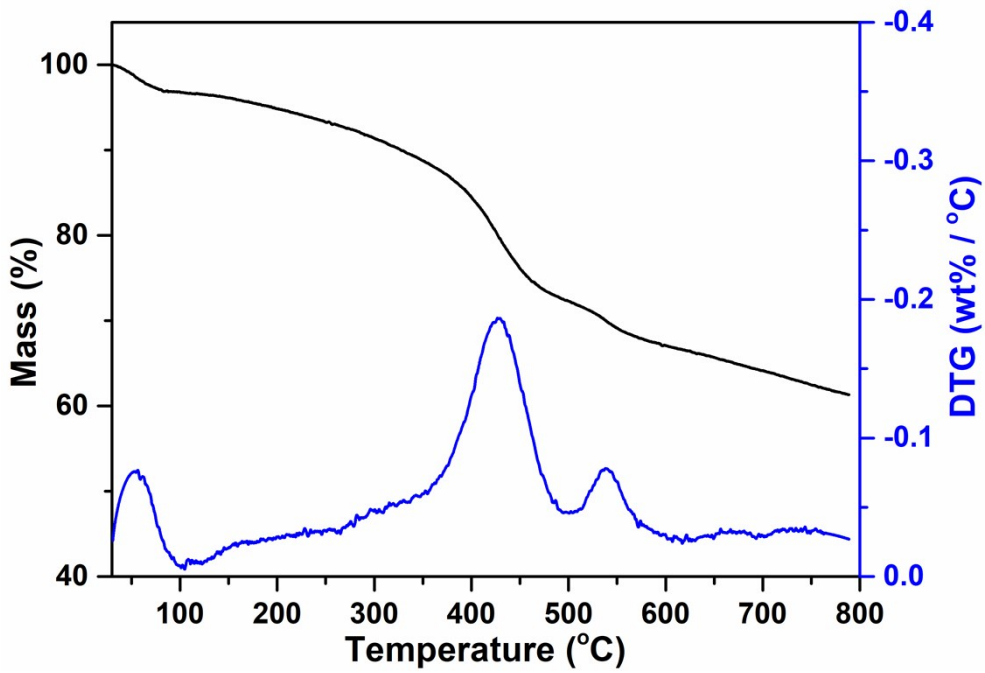

Fig. S21. TG and DTG plots of Pd@OFM-1.

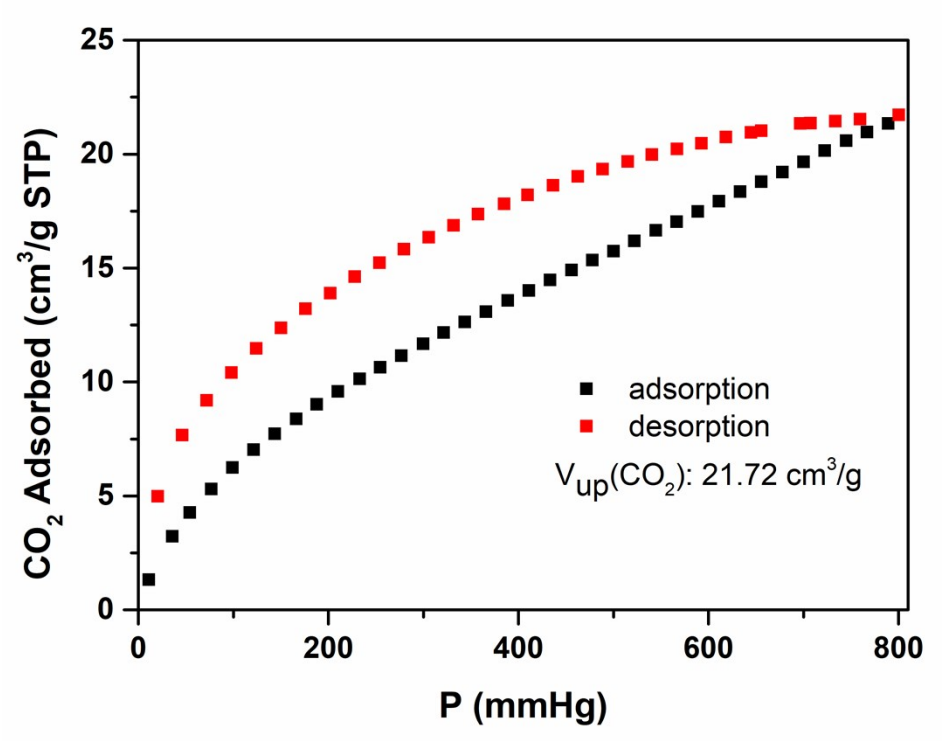

Fig. S22. CO_2 adsorption/desorption isotherms for Pd@OFM-1 at 273 K. The decreased CO_2 uptakes should be ascribed to encapsulation of the Pd nanoparticles inside the pore space of OFM-1.

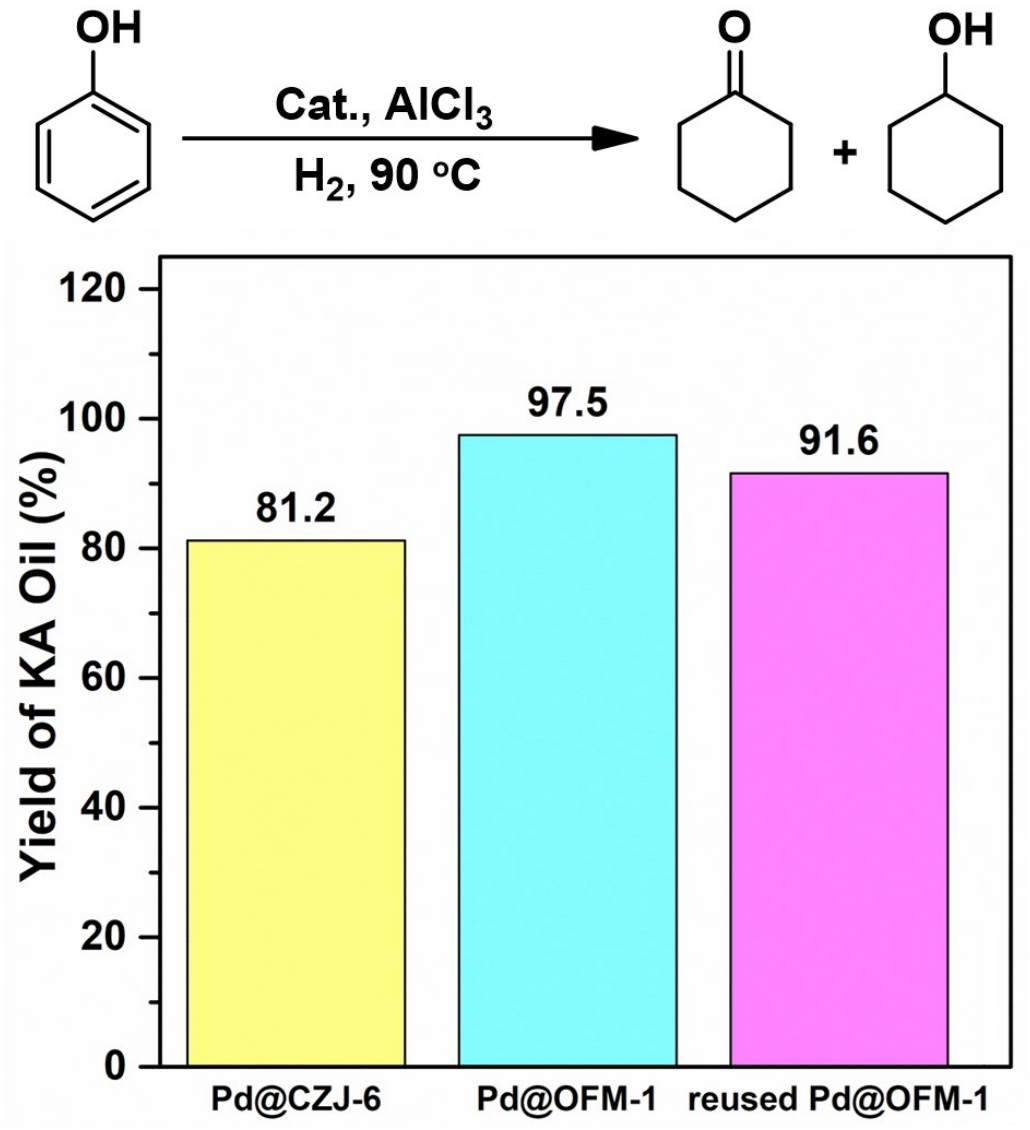

Fig. S23. Catalytic performances of different catalysts for phenol hydrogenation reaction.

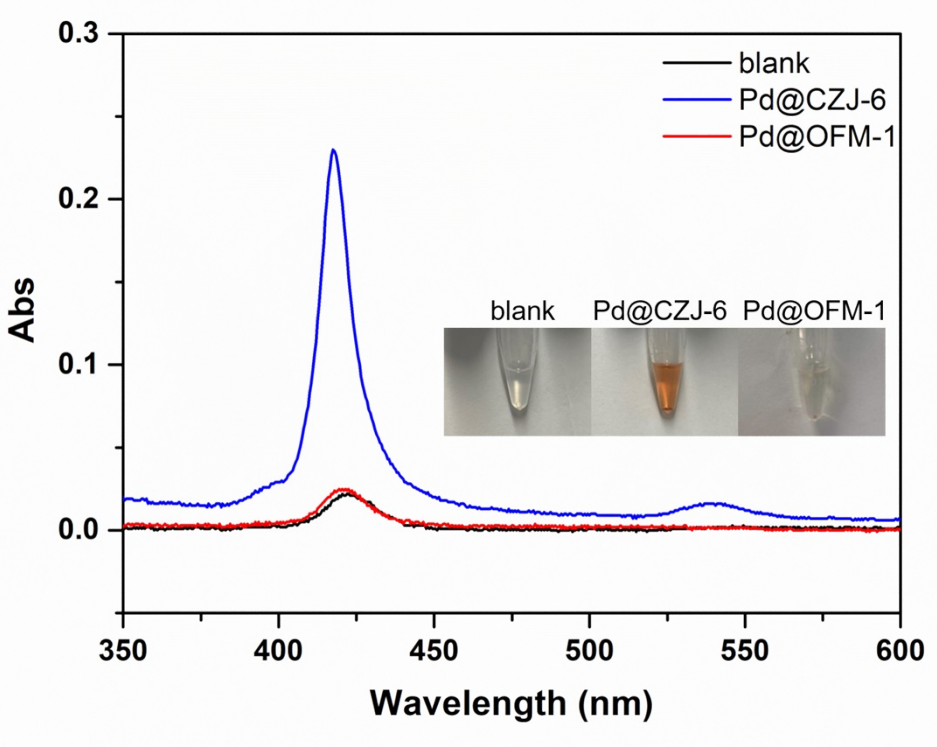

Fig. S24. UV-vis absorption spectra and digital photographs of ethyl acetate extractions of the reaction mixtures for blank, Pd@CZJ-6 and Pd@OFM-1 after catalysis.

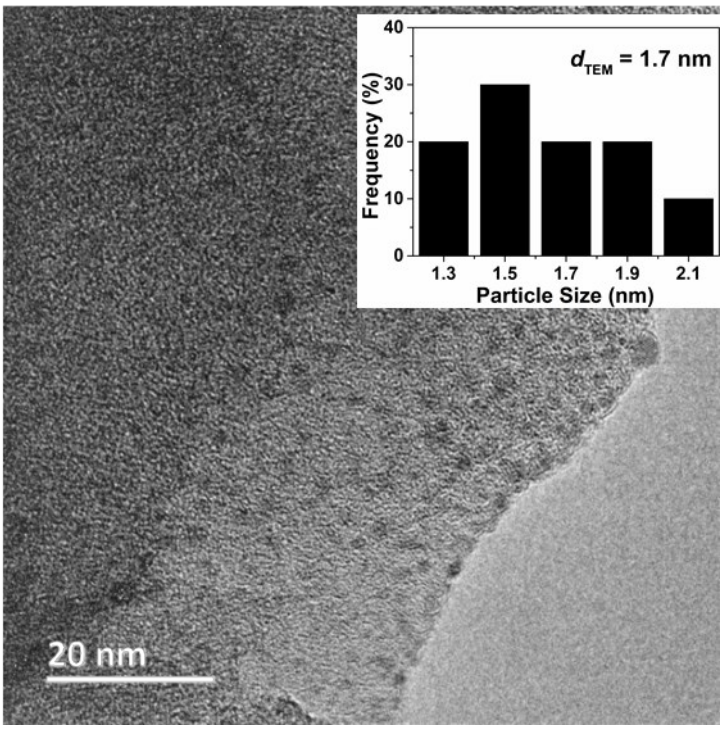

Fig. S25. HRTEM image of Pd@OFM-1 after catalysis.

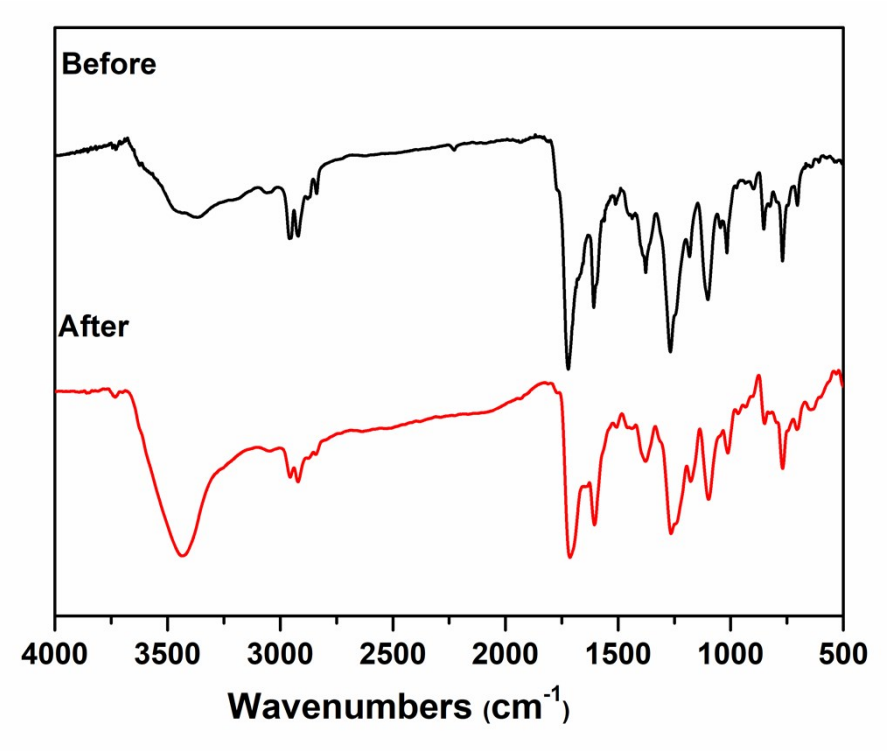

Fig. S26. FT-IR spectra of Pd@OFM-1 before and after catalysis.

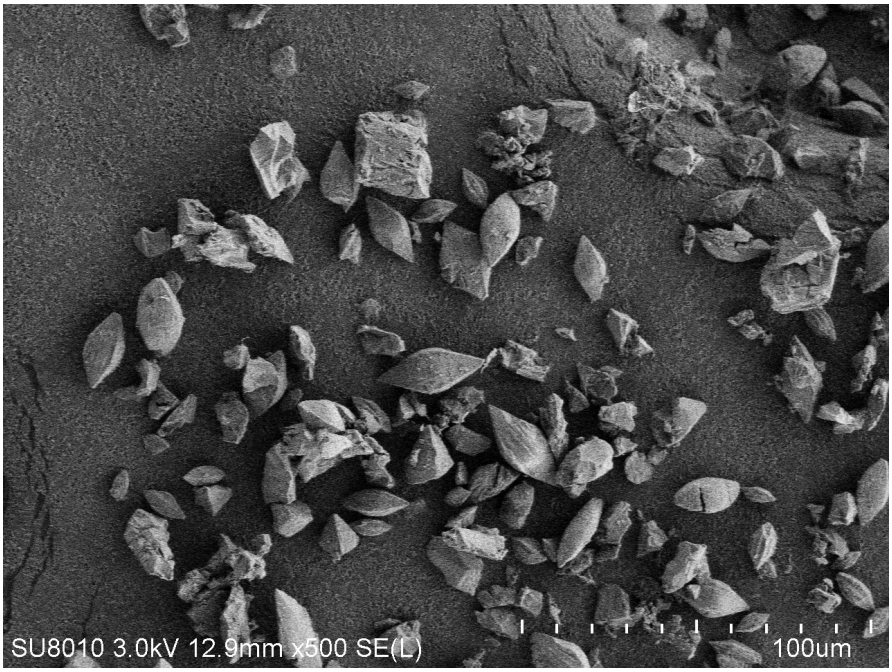

Fig. S27. SEM image of Pd@OFM-1 after catalysis.

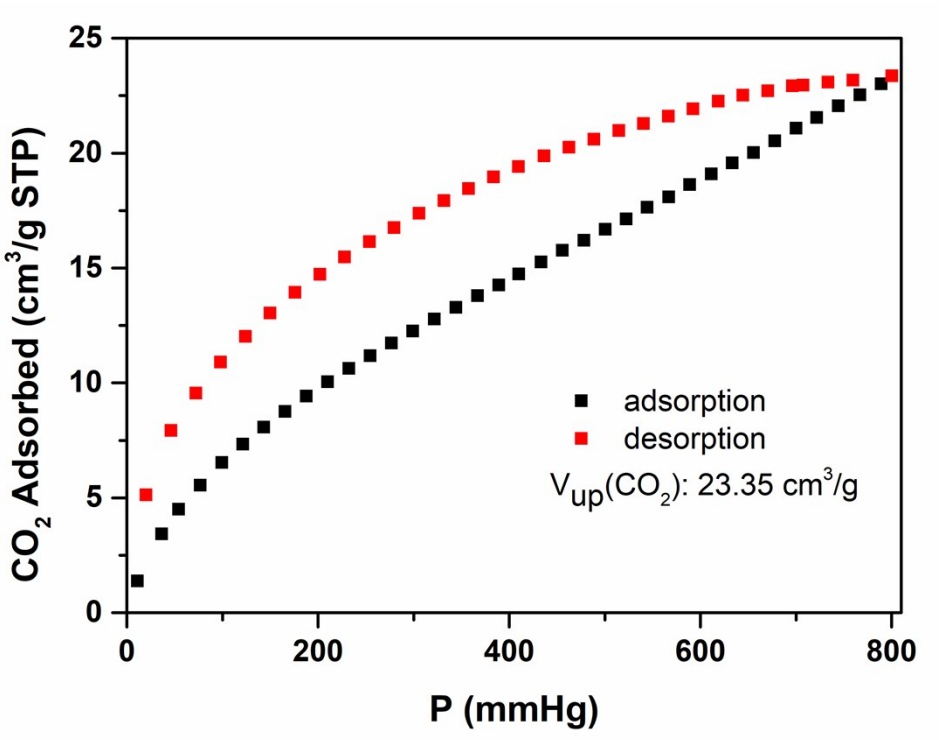

Fig. S28. CO_2 adsorption/desorption isotherms for Pd@OFM-1 after catalysis at 273 K.

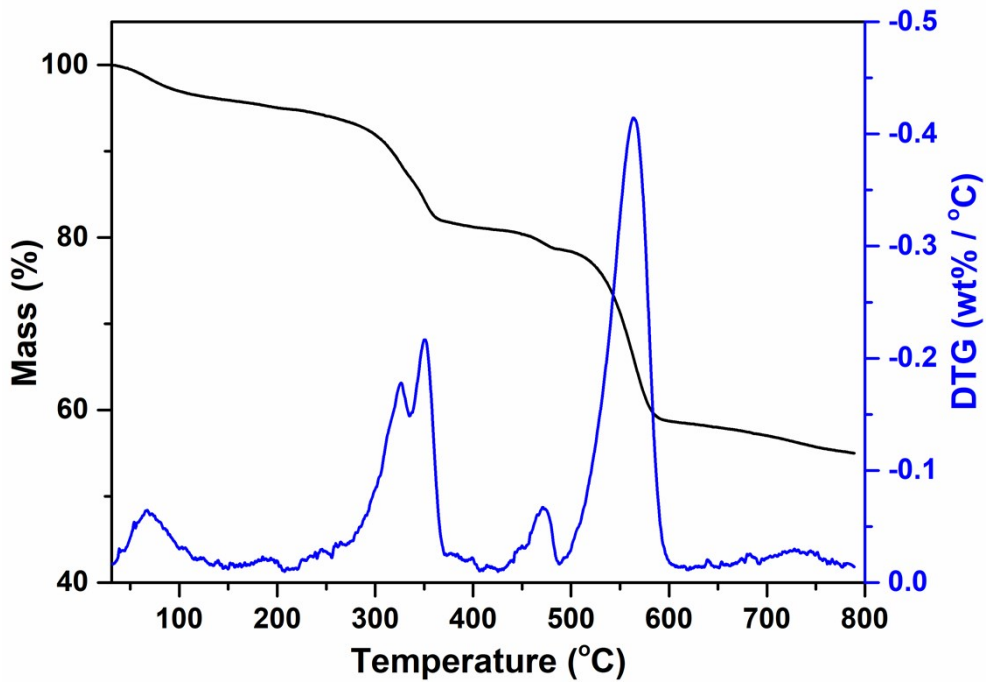

Fig. S29. TG and DTG plots of Pd@CZJ-6.

Fig. S30. SEM image of Pd@CZJ-6.

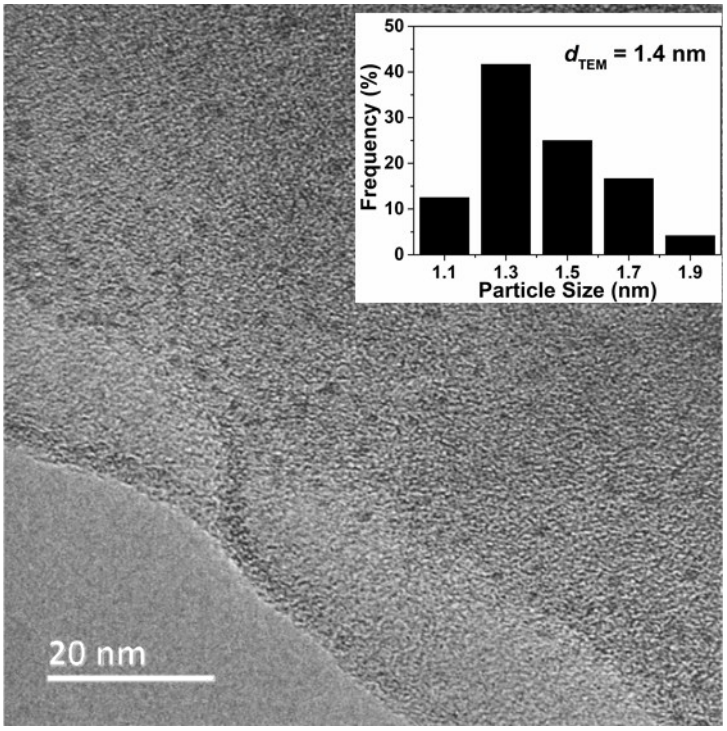

Fig. S31. HRTEM image of Pd@CZJ-6.

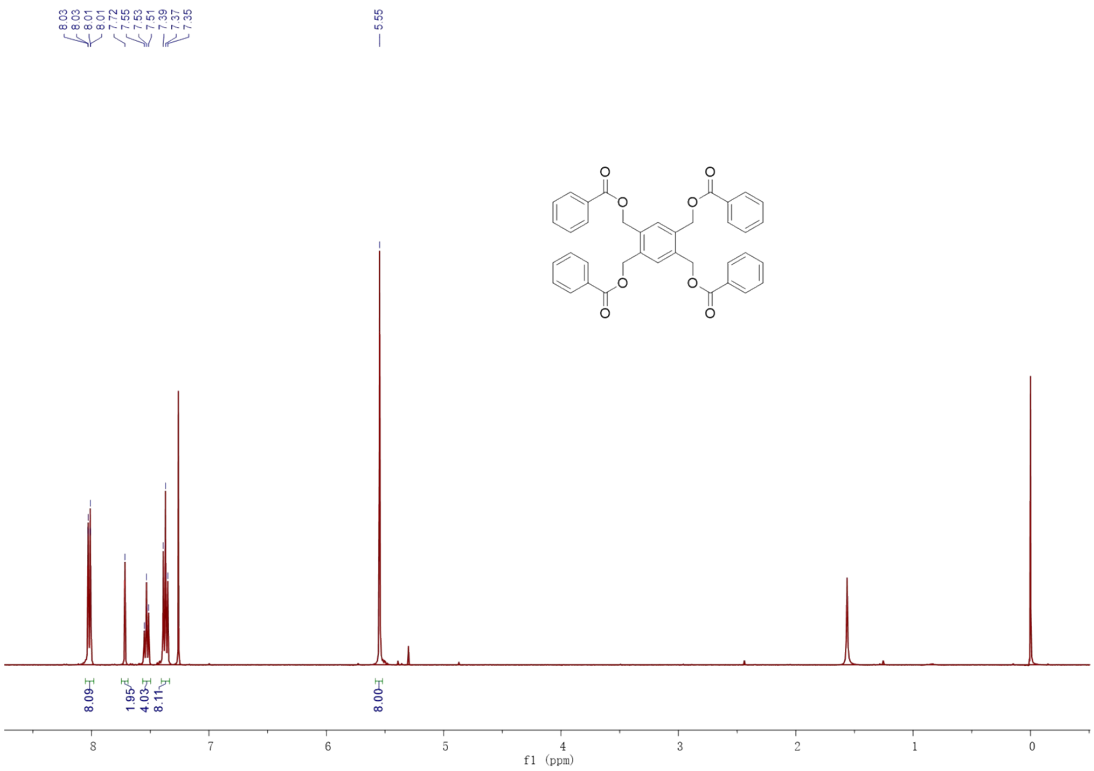

Fig. S32. ^{1}H NMR spectrum of benzene-1,2,4,5-tetrayltetrakis(methylene) tetrabenzoate in $CDCl_3$.

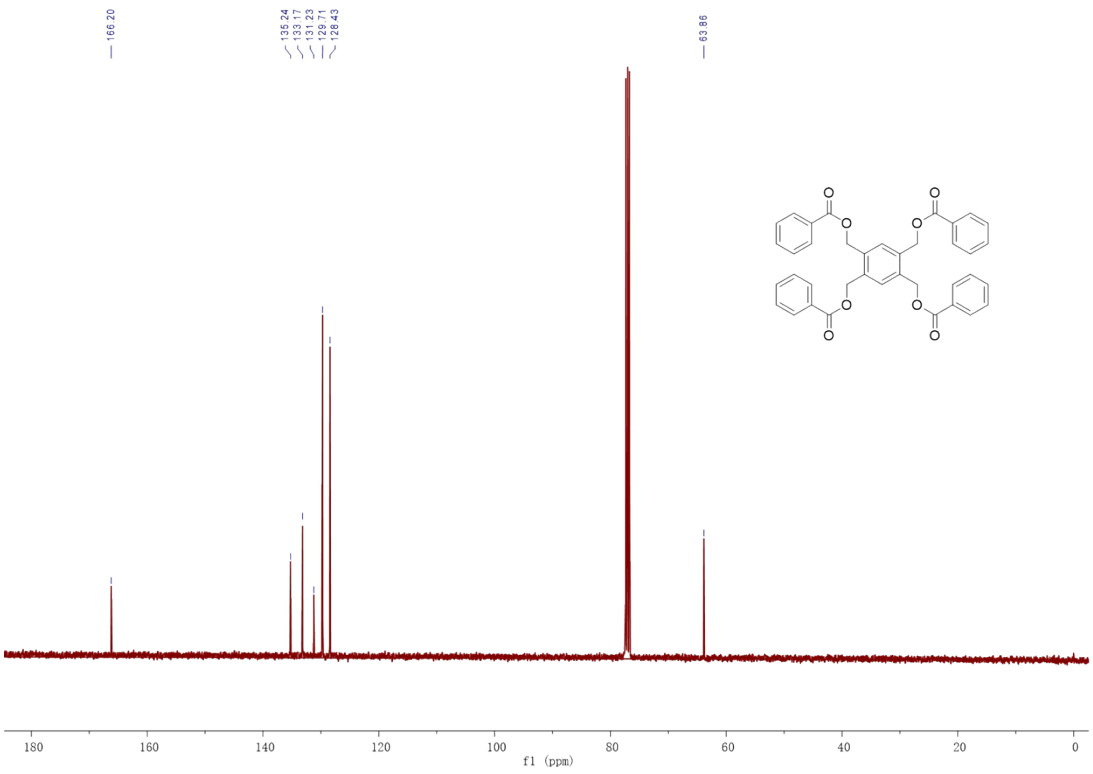

Fig. S33. ^{13}C NMR spectrum of benzene-1,2,4,5-tetrayltetrakis(methylene) tetrabenzoate in $CDCl_3$.

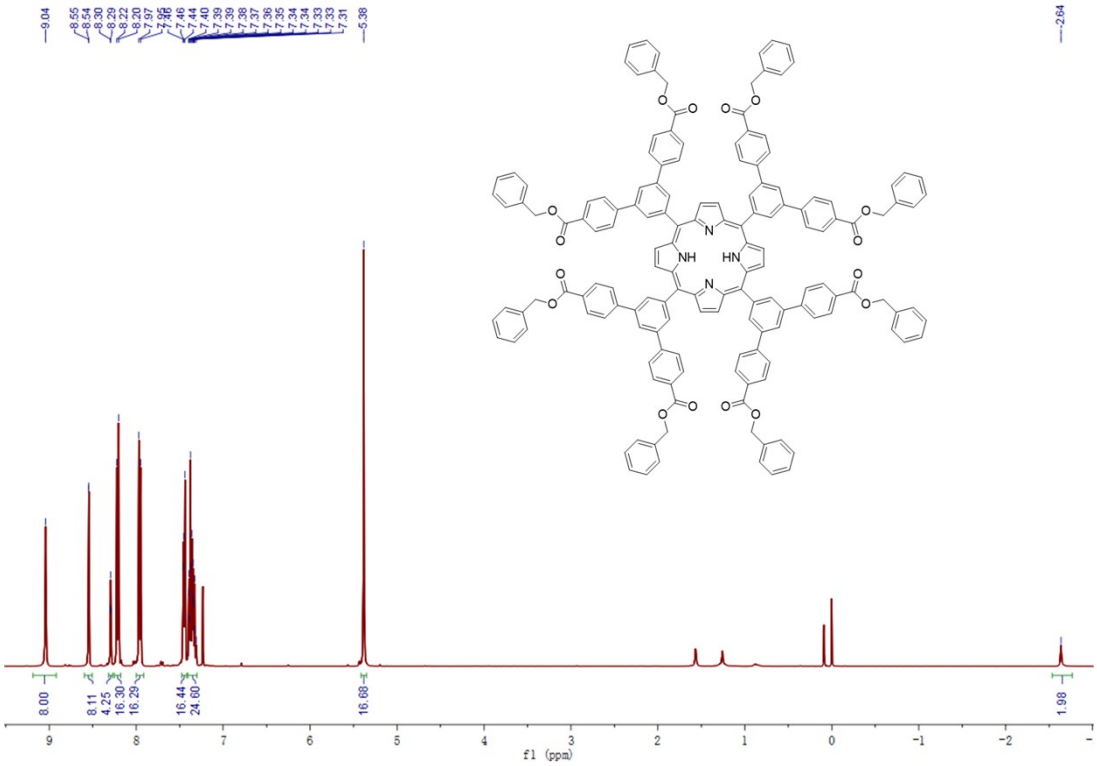

Fig. S34. ^{1}H NMR spectrum of TBPP in $CDCl_3$.

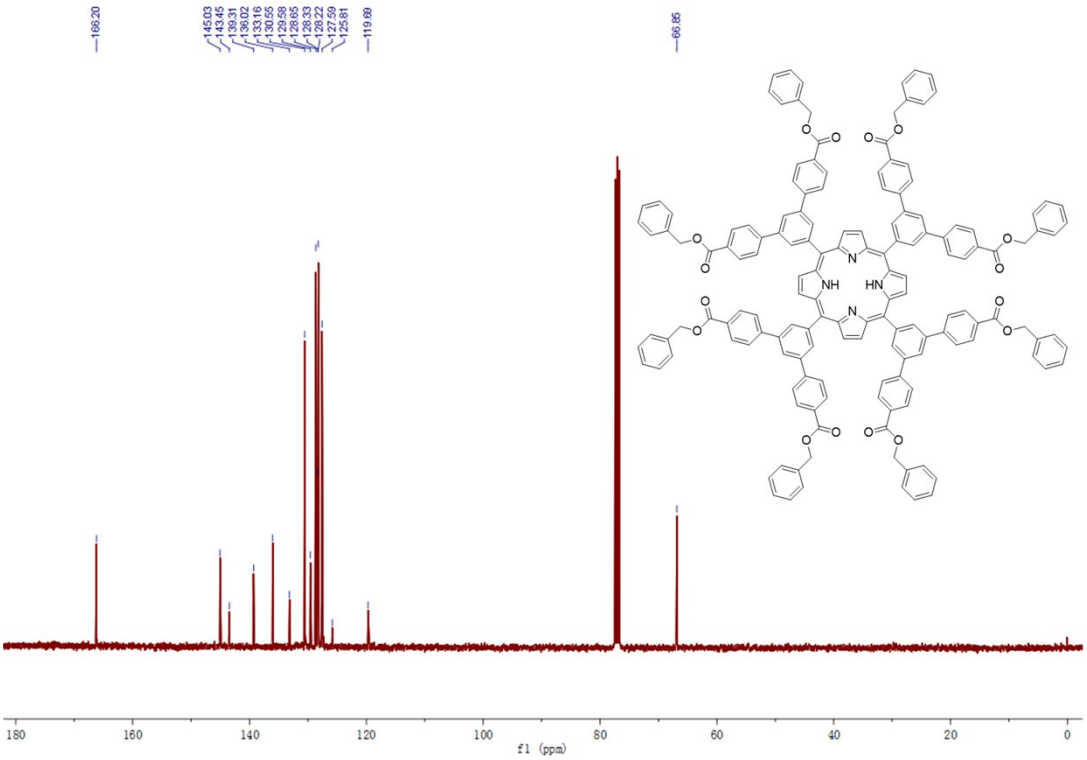

Fig. S35. ^{13}C NMR spectrum of TBPP in $CDCl_3$.

Table S1. Comparison of different catalysts used in the phenol hydrogenation.

Catalyst	P_{H2} (MPa)	Yield (%)	T (°C)	Ref.
Pd/MIL-53	0.5	45.7	50	S4
Pd/MIL-101	0.5	85	50	S4
Pd/C-com	0.5	100	100	S5
Pd/Al-MCM-41	4	98.4	50	S6
Pd/MOF140-AA	2	54.4	260	S7
Pd/C	1	>99.9	30	S8
Pd@mpg-C_3N_4	0.1	>99	100	S9
$Pd^{2.5}$@FDU^{3}–N^{H}	0.1	99	100	S10
Pd/Al_2O_3-3	0.1	>99	60	S11
Pd@sMMT-1	0.1	>99	35	S12
0.5% PdNPs@CNCs	0.4	90	r.t.	S13
Pd@CN_{600}	0.1	98.1	80	S14
Pd@hydrophilic-C	1	>99	100	S15
Pd@OFM-1	1	97.5	90	This work

References

[S1] M. Zhao and C.-D. Wu, *ChemCatChem*, 2017, **9**, 1192.

[S2] M.-J. Dong, X. Wang and C.-D. Wu, *Adv. Funct. Mater.,* 2019, **30**, 1908519.

[S3] A. F. Lee, S. F. Hackett, J. S. Hargreaves and K. Wilson, *Green Chem.,* 2006, **8**, 549.

[S4] D. Zhang, Y. Guan, E. J.M. Hensen, L. Chen and Y. Wang, *Catal. Commun.,* 2013, **41**, 47.

[S5] Y. Pérez, M. Fajardo and A. Corma, *Catal. Commun.,* 2011, **12**, 1071.

[S6] M. Chatterjee, H. Kawanami, M. Sato, A. Chatterjee, T. Yokoyama and T. Suzuki, *Adv. Synth. Catal.,* 2009, **351**, 1912.

[S7] H. Chen, Y. He, L. D. Pfefferle, W. Pu, Y. Wu and S. Qi, *ChemCatChem,* 2018, **10**, 2558.

[S8] H. Liu, T. Jiang, B. Han, S. Liang and Y. Zhou, *Science,* 2009, **326**, 1250.

[S9] Y. Wang, J. Yao, H. Li, D. Su and M. Antonietti, *J. Am. Chem. Soc.,* 2011, **133**, 2362.

[S10] Z. Li, J. Liu, C. Xia and F. Li, *ACS Catal.,* 2013, **3**, 2440.

[S11] L. Cheng, Q. Dai, H. Li and X. Wang, *Catal. Commun.,* 2014, **57**, 23.

[S12] C.-J. Lin, S.-H. Huang, N.-C. Lai and C.-M. Yang, *ACS Catal.,* 2015, **5**, 4121.

[S13] C. M. Cirtiu, A. F. Dunlop-Brière and A. Moores, *Green Chem.,* 2011, **13**, 288.

[S14] S. Ding, C. Zhang, Y. Liu, H. Jiang, W. Xing and R. Chen, *J. Ind. Eng. Chem.,* 2017, **46**, 258.

[S15] P. Makowski, R. D. Cakan, M. Antonietti, F. Goettmann and M.-M. Titirici, *Chem. Commun.,* 2008, **8**, 999.